SUPLEMENTARY SECTION

1. Structural characterization

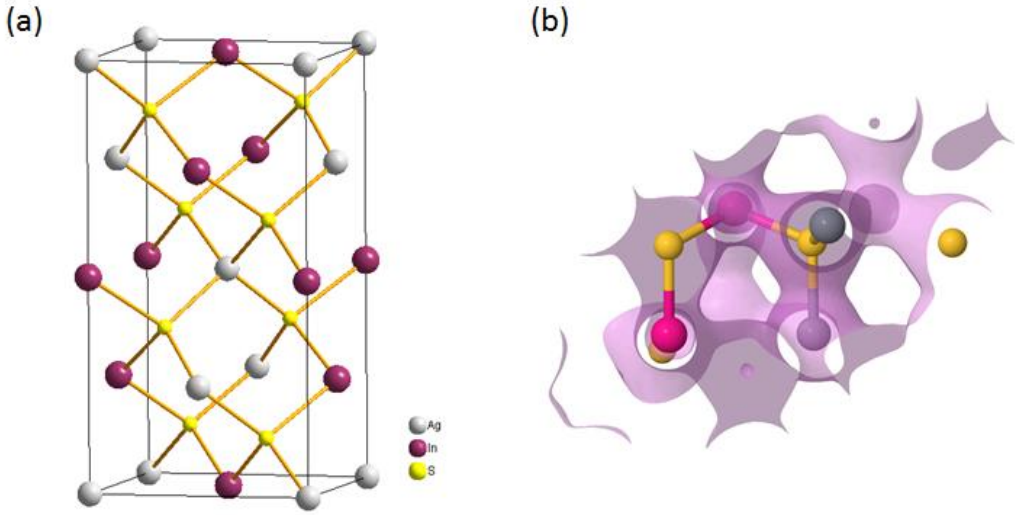

Figure 1s (a) Representation of the unit cell of the ternary chalcopyrite $AgInS_2$ structure and the (b) eight atom primitive cell along with the ground state electronic density.

Tab. 1s Structural parameters for the chalcopyrite tetragonal unit and the triclinic primitive cell (see the Fig. 1s) obtained in the framework of DFT calculations. Parameters R_{AX} and R_{BX} denote average bond length between A^I and B^{III} cations and X^{VI} anion in the $A^IB^{III}X^{VI}_2$ structure. Parameters u and η denote the tetrahedral and tetragonal distortions.

	Cell parameters						Bond length			
	a [Å]	b [Å]	c [Å]	α [°]	β [°]	γ [°]	R_{AX} [Å]	R_{BX} [Å]	u	η
Prim. cell	6.7161	6.7161	6.7161	130.156	130.156	73.157	2.51723	2.31675	n.a.	
Unit cell	5.6601	5.6601	10.7865	90.0	90.0	90.0	2.51723	2.31675	0.2197	0.95285

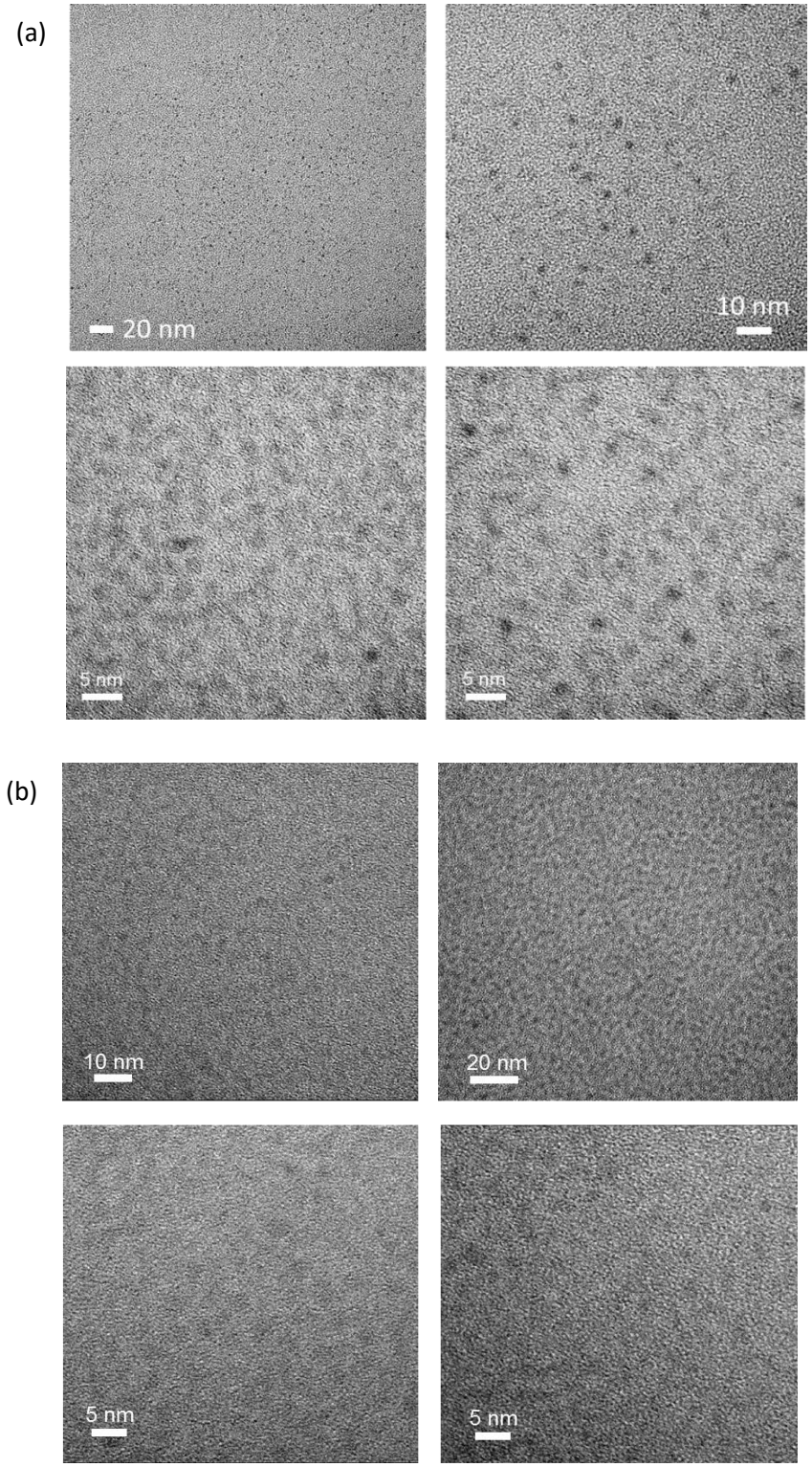

Figure 2s Transmission electron microscopy images of the (a) $AgInS_2$ and (b) $AgInS_2$/ZnS QDs investigated in this paper.

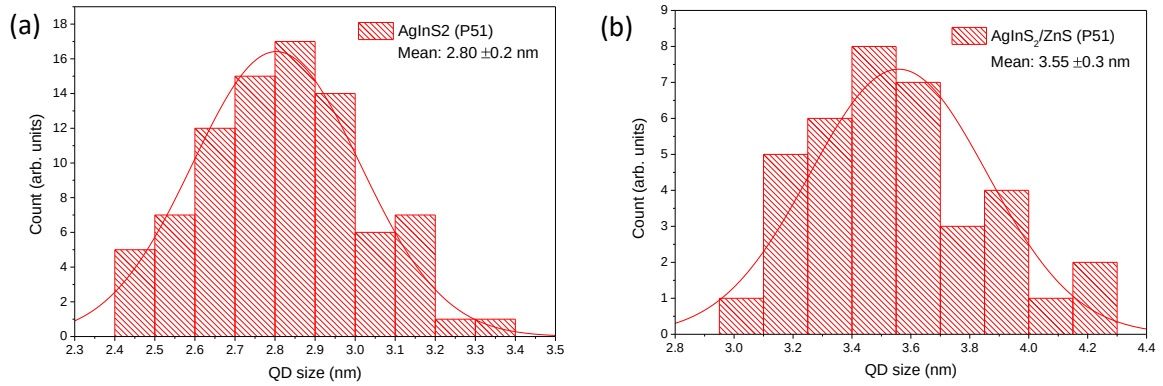

Figure 3s Representative distribution of the (a) $AgInS_2$ and their corresponding (b) $AgInS_2$/ZnS quantum dots. Mean size of the QDs along with the standard deviation have been shown in the plots.

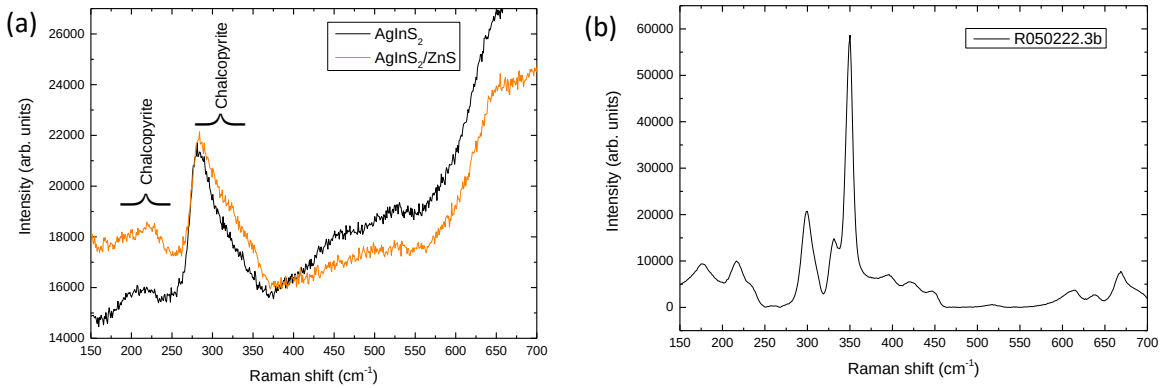

Figure 4s (a) Raman spectra of the $AgInS_2$ (black) and $AgInS_2$/ZnS (orange) QDs. Reference pattern (RRUF database R050222.03) of the chalcopyrite modes have been shown in the figure (b).

2. Electronic band structure and effective masses calculation

Computational details

Calculations of the ground-state properties of the $AgInS_2$ crystal were performed on the basis of density functional theory (DFT) within the projector augmented wave (PAW) approximation as implemented in the ABINIT software package. The Perdew-Wang with local density approximation (LDA) exchange-correlation (XC) energy functionals were used.

The valence structure of Ag, In and S atoms was $[Kr]5s^14d^{10}$, $[Kr]5s^24d^{10}5p^1$, $[Ne]3s^23p^4$ with 11, 13 and 6 valence electrons respectively. The Brillouin zone of the primitive unit cell was sampled on the 8 × 8 × 8 Monkhorst-Pack k-point grid. The PAW cut-off energy was 15 Ha providing convergence of the total energy. Due to the presence of localized d-electron states and its impact on the eigenvalue of the valence band maximum, a Hubbard-like (U = 0.9 eV) correction term was used in the calculations.

Any calculations were performed on structurally optimized models in order to minimize the components of stress tensor below 10^{-5} Ha/Bohr^3.

Due to displacement of anions from their ideal tetrahedral positions, the total energy also converged with respect to the displacement parameter u = 0.27, defining the bond length mismatch $\alpha = (u - ¼)a^2$.

Optical properties of the AIS are based on calculation of the linear response function $\varepsilon(\omega) = \varepsilon_1(\omega) + i\varepsilon_2(\omega)$ in the energy window up to 5 eV.

Calculations of the confined nanostructures were performed using the Gaussian 09 package.[1] Three different hybrid exchange-correlation functionals i.e. B3PW91,[2] B3LYP[3] and HSE06[4] were used in the calculations. The 6-31G all-electron basis set was used to describe the sulfur electrons and SBKJC effective core potential (ECP) with double-ζ basis set[5] for the silver and indium electrons. The basis set and ECP files for Ag and In was taken from EMSL Basis Set Library[6,7]

These particular functional have been used according to Hai et al.[8] reporting previously energy gaps and lattice parameters of 18 bulk ternary semiconductors in chalcopyrite structure and 9 binary semiconductors in zinc blende structure. They have reported very good agreement with experimental results for B3PW91 and B3LYP XC functionals and have compared their results with other results for HSE XC functional.

First results concerning calculations for quantum confined have been performed on a 44 atom $AgInS_2$ cluster cut from an ideal chalcopyrite crystal structure. Before any calculations, the geometry of the nanocrystal was optimized within the Berny algorithm. The optimization was carried out until the convergence of optimization criteria was obtained. The optimization criteria was the maximum force on atoms, RMS (root mean square) force on all atoms, maximum displacement of atom and RMS change of all structural parameters. The values of this criteria were respectively $4.5\cdot10^{-4}$, $3\cdot10^{-4}$, $1.8\cdot10^{-3}$ and $1.2\cdot10^{-3}$, all in atomic units. The energy in every SCF cycle was converged to 10^{-6} Hartree.

The one-electron Kohn-Sham band structure of the $A^{I}B^{III}X^{VI}_2$ AIS crystal as well as the unit cell with corresponding Brillouin-Zone is shown in Fig. 5s. The distinctive feature of the dispersion is the separation of the valence band into four major subbands. The first three subbands are separated by very narrow energy gaps but the fourth band below the valence band maximum (VBM) is separated by energy of 7 eV. The character of the band structure is directly related to the character of structural distortion of the unit cell and displacement of anions from their ideal tetragonal sites as well as the character of the interaction between the noble metal (A^{I}) localized d-states and the sp^3-hybridized anion states. The repelling interaction between the d-p orbitals has to be taken into consideration for proper values of the band gap.

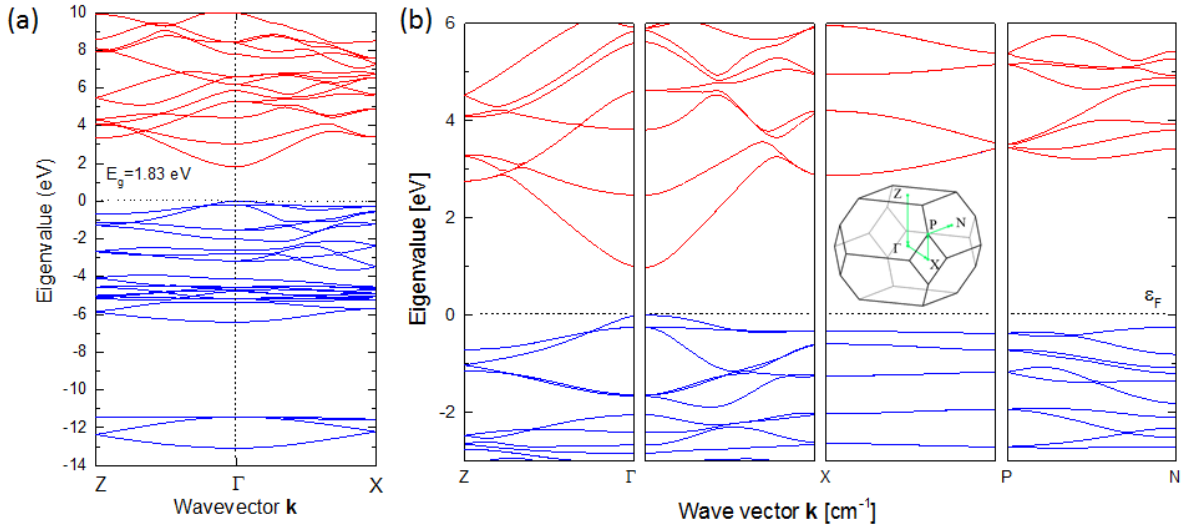

Figure 5s (a, b) Kohn-Sham electronic band structure calculated for the $AgInS_2$ crystal. The fermi energy is represented at the VBM.

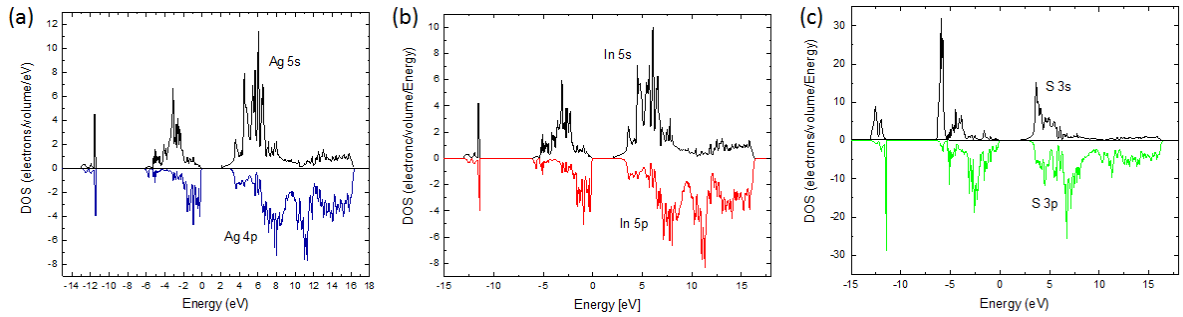

Figure 6s The calculated partial density of states (DOS) for the bulk $AgInS_2$ crystal. Different components of the DOS belonging to (a) silver (Ag), (b) indium (In) and (c) sulfur (S) have been shown at different picture.

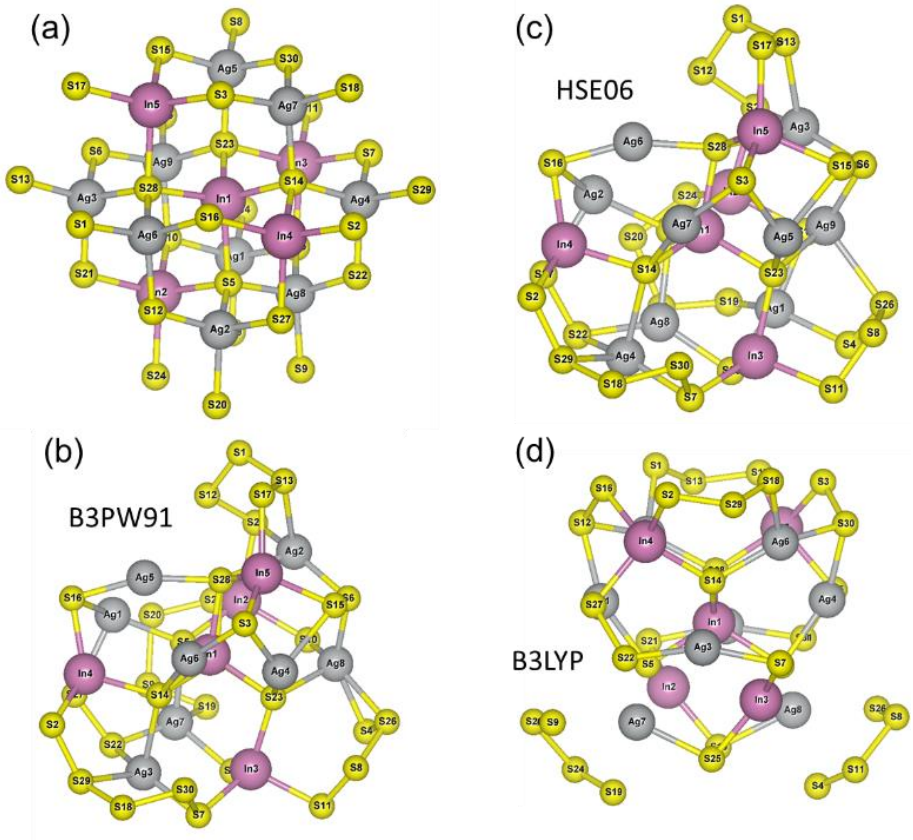

Figure 7s (a) The 44 atom $AgInS_2$ cluster cut directly from an ideal $AgInS_2$ crystal structure. Intentionally the cluster was terminated by the sulfur atoms. In this study, reconstruction of the ideal model was performed with Berny algorithm using three different hybrid functionals (b) B3PW91, (c) HSE06 and the (d) B3LYP. Obtained results of corresponding optimized clusters may be seen in the images.

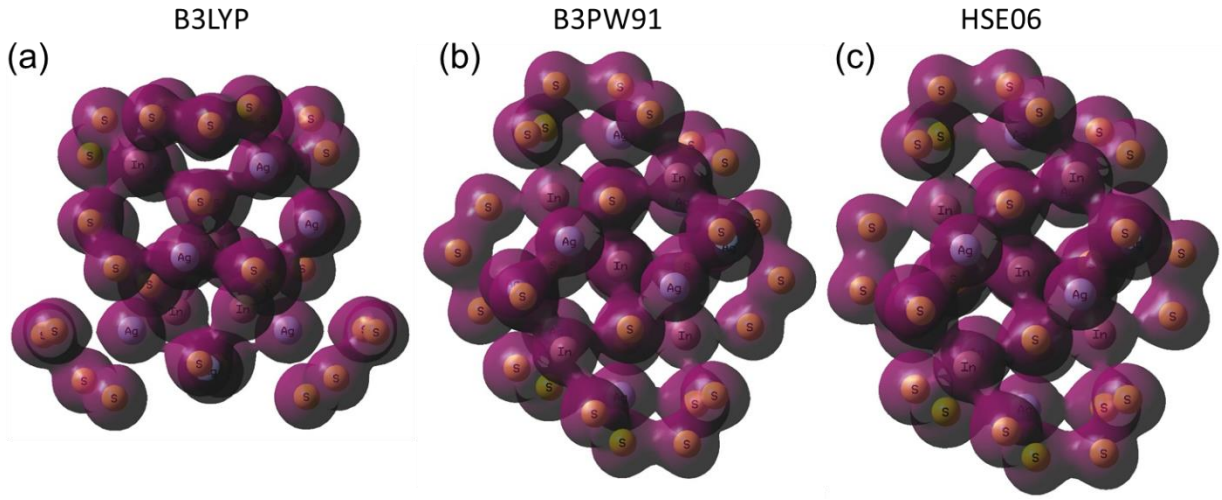

Figure 8s A 3D projection of the electronic density around the clusters optimized by (a) B3LYP, (b) B3PW91 and the (c) HSE06 hybrid functionals. Formation of the S-S disulfide bonds and their higher oligomers is well seen.

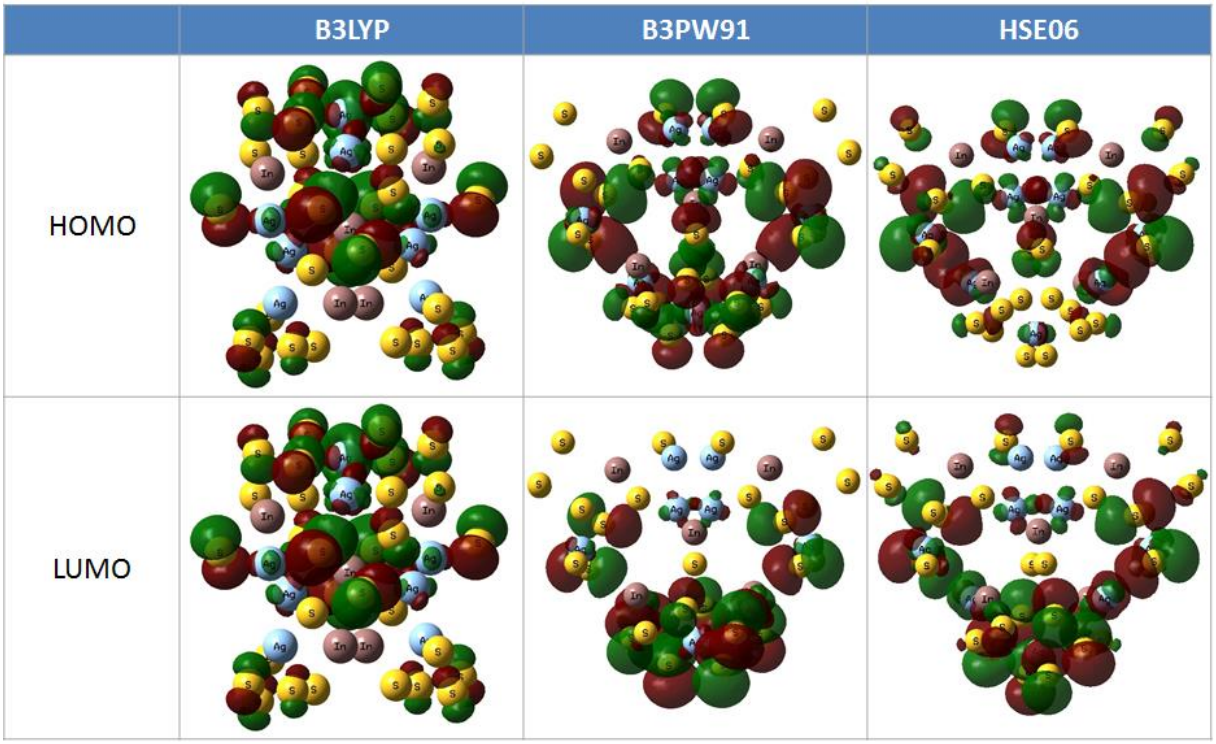

Figure 9s Projections of the highest (HOMO) and lowest (LUMO) occupied states of the 44 atom $AgInS_2$ cluster calculated for the three different hybrid functionals.

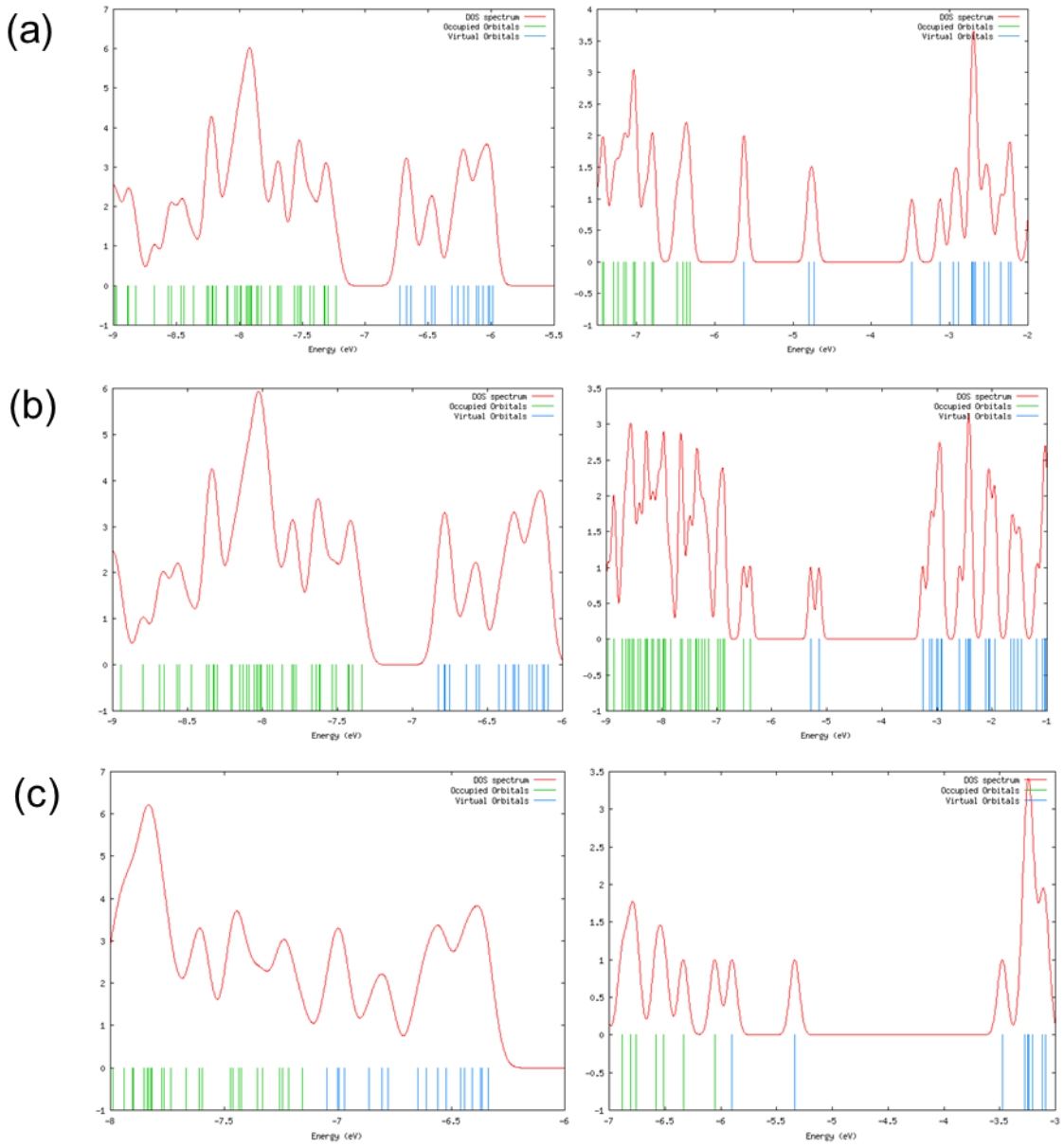

Figure 10s Total density of states (DOS) calculated for the (a) B3LYP, (b) B3PW91 and (c) HSE06 hybrid functionals. The DOS for optimized cluster were shown on the right. On the left side are shown the DOS for unoptimized cluster for reference.

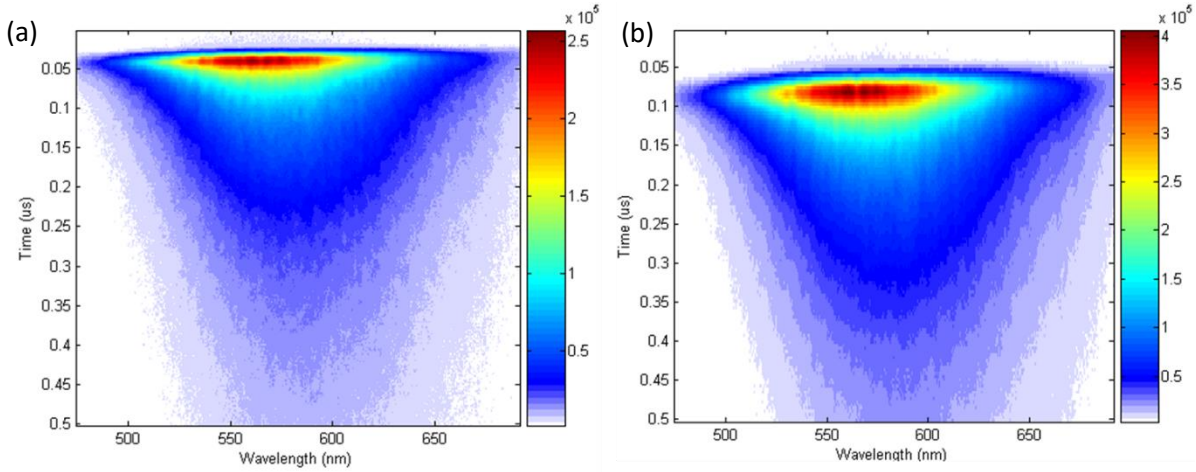

Figure 11s Representative time-resolved photoluminescence (TRPL) spectra of the $AgInS_2$/ZnS QDs (a) without magnetic field and (b) with magnetic field of B = 0.5 T.

References

[1] Gaussian 09, Revision D.01, Frisch, M. J.; Trucks, G. W.; Schlegel, H. B et al. Gaussian, Inc., Wallingford CT, 2009.

[2] Becke, A. (1993). Density Functional Thermochemistry III The Role of Exact Exchange. J. Chem. Phys., 98(7), 5648–5652.

[3] Devlin, F. J., Finley, J. W., Stephens, P. J., & Frisch, M. J. (1995). Ab Initio Calculation of Vibrational Absorption and Circular Dichroism Spectra Using Density Functional Force Fields: A Comparison of Local, Nonlocal, and Hybrid Density Functionals. The Journal of Physical Chemistry, 99(46), 16883–16902.

[4] Krukau, A. V., Vydrov, O. a., Izmaylov, A. F., & Scuseria, G. E. (2006). Influence of the exchange screening parameter on the performance of screened hybrid functionals. The Journal of Chemical Physics, 125(22), 224106.

[5] Stevens, W. J., Krauss, M., Basch, H., & Jasien, P. G. (1992). Relativistic compact effective potentials and efficient, shared-exponent basis sets for the third-, fourth-, and fifth-row atoms. Canadian Journal of Chemistry, 70(2), 612–630.

[6] Feller, D., The Role of Databases in Support of Computational Chemistry Calculations. J. Comp. Chem., 17(13), 1571-1586, 1996.

[7] Schuchardt, K.L., Didier, B.T., Elsethagen, T., Sun, L., Gurumoorthi, V., Chase, J., Li, J., and Windus, T.L. Basis Set Exchange: A Community Database for Computational Sciences. J. Chem. Inf. Model., 47(3), 1045-1052, 2007, doi:10.1021/ci600510j.

[8] Hai, X., Tahir-Kheli, J., & Goddard, W. a. (2011). Accurate band gaps for semiconductors from density functional theory. Journal of Physical Chemistry Letters, 2(3), 212–217. http://doi.org/10.1021/jz101565j